# Volcanic eruption time forecasting using a stochastic enhancement of the Failure Forecast Method

**Andrea Bevilacqua**[1,2,3], Abani Patra[3,4], E. Bruce Pitman[5], Marcus Bursik[2], Flora Giudicepietro[6], Giovanni Macedonio[6], Augusto Neri[1], Greg Valentine[2]

*(1) INGV, Sezione di Pisa, Pisa, Italy; (2) Department of Earth Sciences, UB, Buffalo, NY; (3) Computational Data Sciences and Engineering Program, UB, Buffalo, NY; (4) Department of Mechanical and Aerospace Engineering, UB, Buffalo, NY; (5) Department of Material Design and Innovation, UB, Buffalo, NY; (6) INGV, Osservatorio Vesuviano, Napoli, Italy.*

AGU100 ADVANCING EARTH AND SPACE SCIENCE
FALL MEETING
Washington, D.C. | 10–14 Dec 2018
Paper Number V23G – 0155
Abstract ID: 413317

## 1. Theoretical introduction

The Failure Forecasts method (FFM) is a well-established tool in the interpretation of monitoring data as possible **precursors**, providing quantitative predictions of the eruption onset $t_c$, commonly represented by inverse rate plots (Voight, 1988; 1989 Fig. 1).

The model (Fig. 2) represents the potential cascade of precursory signals leading to a large-scale rupture of materials culminating at the **failure time** $t_f$. The equation was originally developed in landslide forecasting (Fukuzuno, 1985).

FFM has been retrospectively applied to several volcanic systems, including dome forming and **explosive** eruptions (Voight&Cornelius, 1991; Voight et al., 2000). **Seismic** data are the type of signals most extensively studied with the method (Cornelius&Voight, 1994; Ortiz et al., 2003; Budi-Santoso et al., 2013).

Laboratory experiments and theoretical models demonstrated the use of the FFM under **constant stress** and temperature (Hyman et al., 2018). Without this assumption, more fundamental relations between rock fracture and deformation imply time dependent **changes** in the power law properties (Robertson&Kilburn, 2016; Kilburn, 2018).

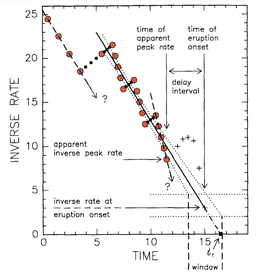


**Fig 1.** Schematic example of linear regression of inverse rate of cascading signals (modified from Cornelius & Voight, 1995)

FFM is known to be affected by sources of **uncertainty**, like:

- the occurrence of multiple phases of acceleration in the signals (Bouè et al., 2015)
- varying stress on the system, or temperature (Kilburn, 2012)
- the superposition of signals originating from different causes (Salvage&Neuberg, 2016)
- heterogeneity in the breaking material, producing changes in the signals (Vasseur et al., 2015).

In addition, the statistical fitting of model parameters can be poorly constrained (Bell et al., 2011).

In this study, we enhance the classical FFM by systematically characterizing the **uncertainty**. We incorporate stochastic **noise** in the equations, and a mean-reversion property to constrain the noise.

We describe three different methods for estimating $t_f$, the ODE-based **Method 1**, the new SDE-based **Method 2**, and their combined doubly stochastic formulation **Method 3**.

**Doubly stochastic** models describe the effect of **epistemic uncertainty** in the formulation of **aleatory processes** (Cox&Isham, 1980; Bevilacqua2016).

We retrospectively test the enhanced FFM over four datasets (Voight, 1988). They refer to: **Mt. St. Helens**, 1981-82 (Swanson,1982), **Bezymyanny**, 1960 (Tokarev, 1966), Mt. Toc, 1963 (Müller, 1964). The last dataset is the landslide above the **Vajont Dam** in Italy (Kilburn&Petley, 2003). Finally we show a preliminary application to present-day earthquake count at **Campi Flegrei** caldera.

### 1.1 CLASSICAL FFM FORMULATION

$$dX/dt = AX^{\alpha}$$ where X is the time rate of signals

α - convexity parameter
A - slope parameter
$t_0$ - initial time

$$X(t) = \left[(1-\alpha)A(t-t_0) + X(t_0)^{1-\alpha}\right]^{\frac{1}{1-\alpha}}$$ SOLUTION

$$\eta := X^{1-\alpha} \quad \xrightarrow[\text{linearization}]{\text{change of variables}} \quad \frac{d\eta}{dt} = (1-\alpha)$$

$$\eta(t) = (1-\alpha)A(t-t_0) + \eta(t_0)$$

**Fig 2.** ODE solution, (a) X, and (b) 1/X. Note the effect of varying slope and convexity parameters α, A learnt from data.

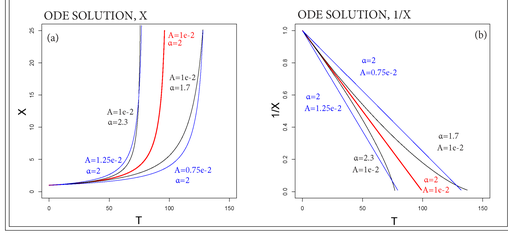


### 1.2 ENHANCED FFM FORMULATION

Our aim is to produce **probability forecasts** with the FFM, instead of deterministic predictions. We embed **noise** in the model and enable sudden changes in the power law properties (Fig. 3).

We assume that the FFM equation is not exactly satisfied, but there is a **transient difference** produced by additive noise, which however decreases exponentially in time. This is called a Hull-White model in finance (Hull&White, 1990).

$$d\eta_t = \underbrace{\{\gamma\left[(1-\alpha)A(t-t_0) + \eta_{t_0} - \eta_t\right]}_{\text{mean-reversion terms}} + \underbrace{(1-\alpha)A\}\,dt}_{\text{classical FFM}} + \underbrace{\sigma dW_t}_{\text{noise term}}$$

The mean-reversion property makes every perturbation decay with time

$$X_t = \left\{X_{t_0}^{1-\alpha} + \int_{t_0}^{t}\{\gamma\left[(1-\alpha)A(s-t_0) + X_{t_0}^{1-\alpha} - X_s^{1-\alpha}\right] + (1-\alpha)A\}\,dt + \int_{t_0}^{t}\sigma dW_s\right\}^{\frac{1}{1-\alpha}}$$ NONLINEAR FORMULATION

γ - mean-reversion parameter
σ - noise parameter
β - initial perturbation

Parameters γ, σ are based on the residuals in the linearized problem.

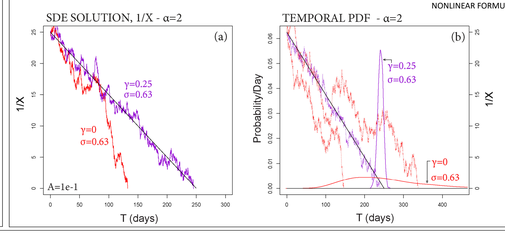


**Fig 3.** SDE solutions, with α=2, A=0.1. The black line is the mean solution. (a) colored lines are SDE paths, γ=0 or γ=0.25. (b) also shows $g_{tf}$. 1/X is reported again.

**PROBABILISTIC FAILURE TIME**

$$t_f(\omega) = \inf\{t : X^{-1}(\omega, t) = 0\}$$

random variable

$$g_{t_f} : \mathbb{R} \to \mathbb{R}+$$

$t_f$ probability density function

## 2. Example of retrospective estimators

Log-rate vs Log-acceleration Technique (LLT), and Hindsight Technique (HT) are classical estimators of α (Cornelius & Voight, 1995). LLT is less accurate than HT and needs a second order derivative of data. HT needs to know $t_c$ and can only be used retrospectively.

**Fig 4,5,6.** Estimators of $t_f$ based on Method 1 (Fig. 4), Method 2 (Fig. 5), and Method 3 (Fig. 6).

Blue lines assume α as from LLT, red as from HT. The bold line is $g_{tf}$, the probability/day scale bar is related to it. In Fig.6 bold dashed lines are its 5th and 95th percentile values.

Thin dashed lines bound the 90% confidence interval of the ODE paths of 1/X, and a thin continuous line is the mean path.

Black points are inverse rate data.

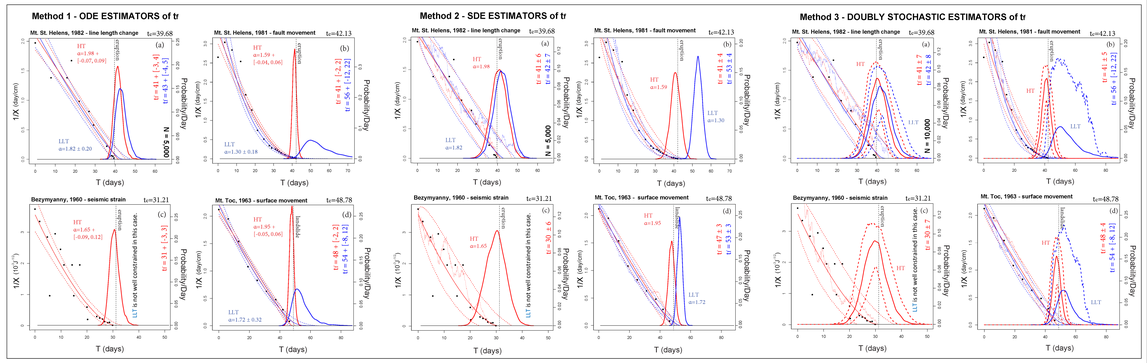


We apply three different forecast methods on the datasets in Voight, (1988), and we test $t_f$ as an estimator of $t_c$.

- Method 1 (Fig. 4) characterizes the **epistemic uncertainty** related to the parameter fitting in the classical FFM. We sample a multivariate Gaussian in a Monte Carlo simulation of 5,000 samples.
- Method 2 (Fig. 5) allows **excursions** from the classical FFM solutions, modeled as **aleatoric uncertainty** sources. The numerical solution of the SDE is performed as 5,000 discretized random paths by the Euler-Maruyama method.
- Method 3 (Fig. 6) combines the other methods. The mean solution is affected first by the parameter uncertainty and then perturbed by the stochastic noise. $g_{tf}$ is reported as 5th percentile, mean, and 95th percentile curves. Mean is based on 10,000 samples. Percentile values on 60,000 samples.

When **α ≈ 2**, all methods provide good estimators of $t_c$. When α < 1.6, Method 1 can overestimate $t_c$ . Noise reduces this issue and can push 1/X to zero earlier. Method 3 performs well, and its formulation allows users to determine a "**worst case scenario"** with a specified level of confidence .

If α is based on LLT Method 1 provides low likelihoods, below 1% in some case (Fig. 7). The 95th percentile values of Method 3 clearly **outperform** other methods. We remark that the HT method cannot be used in forward forecasting, but only retrospectively.

**Fig 7.** Column plots of the likelihood $g_{tf}(t_c)$, i.e. the probability of failure time $t_f$ in the correct day $t_c$. In plot (a) the black bars assume Method 1, the colored bars Method 2. Plot (b) assumes Method 3, and the full bars are the mean values, and the shaded bars are the 95th percentile values of the likelihood.

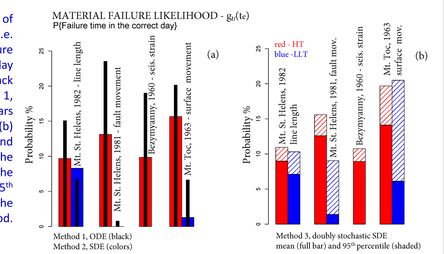


## 3. Probability forecasts on historical datasets

**Fig 8,9,10.** Forecasts of $t_f$ based on Method 1 (Fig. 8), Method 2 (Fig. 9), and Method 3 (Fig. 10).

In (a,b) and (d,e) two examples are tested on different time windows T.

The bold line is $g_{tf}$, the probability/day scale bar is related to it. In Fig.6 bold dashed lines are its 5th and 95th percentile values.

Thin dashed lines bound the 90% confidence interval of the ODE paths of 1/X, and a thin line is the mean path.

Points are inverse rate data, those in T are colored.

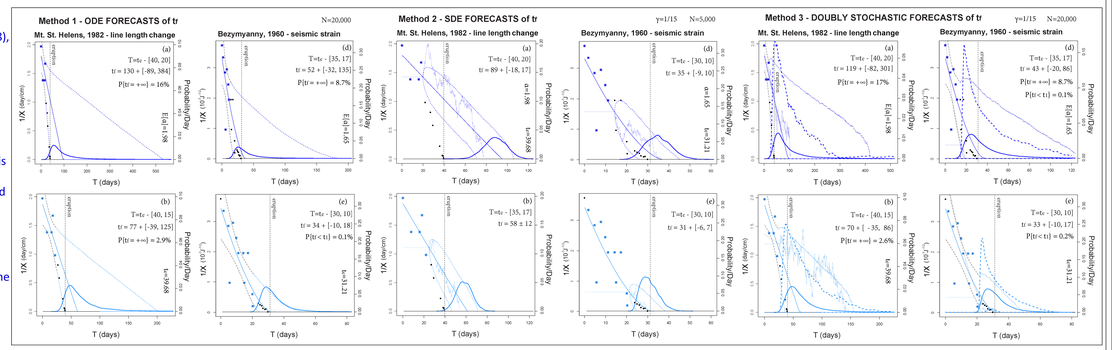


Estimators based on the whole sequence of signals are not **forecasts**. We display forecasts of $t_c$ obtained from parameters inferred from the data collected in a limited time window T=[$t_2$,$t_1$]. For simplicity, α is still based on the entire sequence of processed data in Voight, (1988).

Method 1 (Fig. 8) and mean pdf in Method 3 simulate 20,000 samples, Method 2 (Fig. 9) is based on 5,000 random walks. The percentile values in Method 3 (Fig. 10) are based on 150,000 samples

We compare two **time windows** with extremes reported in figure. They include different subsequences of data. Forecasts can be significantly uncertain, because based on **fewer data**. In Methods 1 and 3, there is a chance that the solution path never hits the real axis.

When the forecast is poorly constrained, Method 2 typically **reduces the uncertainty** affecting $t_f$, compared to Method 1. It tends to give a correct forecast only when the eruption is close. The **doubly stochastic** formulation of Method 3 appears to have an impact.

Method 3 mean forecasts provide consistent likelihoods with Method 1 (Fig. 11). The 95th percentile values are **significantly higher** than other forecasts, from 5% to 10% in the first and second time windows, and above 15% in the third.

We assume **γ=1/15 days**. This is a choice based on the empirical observation that the total length of temporal sequence is at the scale of 45 days, and the duration of well-aligned observations is at the scale of 15 days. Doubled or halved γ produced **minor effects** on the results.

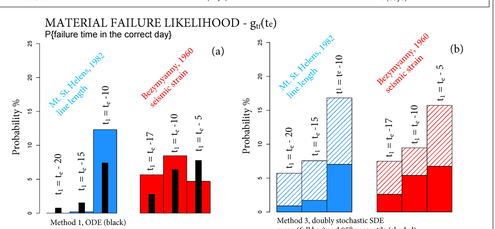


**Fig 11.** Column plots of the likelihood $g_{tf}(t_c)$, in two forecasting examples, on three different time windows. In plot (a) the black bars assume Method 1, the colored bars Method 2. Plot (b) assumes Method 3, and the full bars are the mean values, and the shaded bars are the 95th percentile values of the likelihood.

## 4. Preliminary application to present-day unrest

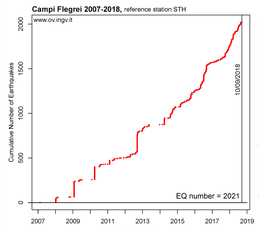


**Fig 12.** Cumulative number of earthquakes measured in Campi Flegrei (Italy) from 1st Jan 2007 to10th Sep 2018. STH station, Agnano.

Campi Flegrei caldera is characterized by **prolonged unrest**. Since 1950, it has undergone **four episodes** of caldera-wide uplift and seismicity, which raised the central region by 4.5 m (Troise et al., 2019).

After about 20 years of subsidence, following the uplift peak reached in 1984, the caldera started a new, **low rate uplift** episode, accompanied by low magnitude **increasing seismicity** (Fig. 12) and marked geochemical changes in fumaroles. Although the interpretation of the current unrest is a matter of debate, Campi Flegrei may be evolving towards conditions more favorable to eruption (Kilburn et al., 2017)

We focus on the **earthquake count** after 2007, available on www.ov.ingv.it. Seismicity is characterized by repeated swarms, superimposed on a background rate (Chiodini et al., 2017). Swarms are believed to be related to fluid-transfer episodes (D'Auria et al., 2011). Further analysis may test the effect of separating the **swarms** from background rate.

In Figure 13 we test our Method 3 on this seismic dataset. We remark that the time window is much longer than in the classical applications, and **spans over 50 years**.

The interpretation of $t_f$ as the onset of a volcanic eruption is purely **speculative**. However, it is the time when **accelerating signals** as observed in the last 10 years will diverge to infinity. A few **pauses** in the seismic rate are filtered out, and are reported in Fig.13a,c. Locally decreasing rates prevent the LLT to calculate α, and we **uniformly sampled α** in [1.4, 2.0]. Here γ = 1/120 days.

Estimates of $t_f$ are in [2019, 2032] with 90% chance, at the scale of 0.02% probability per day. These are **robust** against the choice of the bin on which the rate is calculated (Fig. 13a,b). However, if we consider only the last 5 years, they become sensitive to that choice.

**Fig 13.** Forecasts of $t_f$ based on Method 3. In (a,b) based on the data of 2008-2018, in (c,d) 2013-2018. In (a,c) the inverse rate is obtained on 120 days, in (b,d) on 360 days. Red points are inverse rate data.

The green line is mean value of $g_{tf}$, the probability/day scale bar is related to it. Dashed lines mark its 5th and 95th percentiles.

Thin blue dashed lines bound the 90% confidence interval of the ODE paths of 1/X, and a thin line is the mean path. Grey dotted liner display 50 sample paths of the SDE solution after 10 Sep 18.

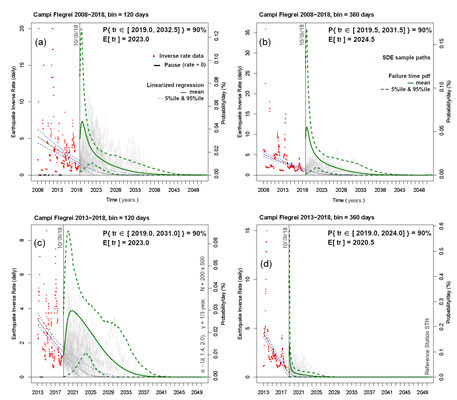


## 5. Conclusions

We have introduced a new method for performing **short-term** eruption forecasting, when eruption onset is related to a rupture of materials.

- The method enhances the well known FFM equation. We allow random excursions from the classical solutions. This provides **probabilistic forecasts** instead of deterministic predictions, giving the user critical insight into a range of failure or eruption dates, and allowing retrospective evaluation and improvement of forecasting methodology.
- Our doubly stochastic formulation can consider the "**worst case scenario"** with a probability of occurrence of at least 5%. This was not possible in the classical formulation.
- We tested the method on historical datasets of precursory signals. The data show the **increased forecasting skill** of the doubly stochastic formulation, expressed as the likelihood in the day of the actual eruption.
- We also described an assessment of failure time on **present-day unrest** signals. The new formulation enables the estimation on longer time windows of data, locally including the effects of variable dynamics.

This approach is the subject of ongoing and future work, with the purpose to further testing forecasting robustness, for example, exploring the sensitivity on a **linear evolution** of α with time, or a more **general structure** of the noise.

***Acknowledgements***: We would like to thank Barry Voight for thoughtful discussions and inspiration, and Christopher Kilburn for having helped us to improve the presentation of the Science. This work is supported by National Science Foundation awards 1339765, 1521855, 1621853 and 1821311, and by Italian Ministry of Education, University, and Research, project FISR2017 - SOIR.

**References:**

***Doubly stochastic enhancement of the Failure Forecast Method using a noisy mean-reverting process and application to volcanic eruption forecasts, https://arxiv.org/abs/1805.11654.***

Bell, A. F., et al. (2011). Geophysical Research Letters, 38(15):5.
Bevilacqua, A. (2016). Theses, 21. Edizioni della Normale, Birkhäuser/Springer.
Boué, A., et al. (2015). Journal of Geophysical Research: Solid Earth, 120(4):2143-2161.
Budi-Santoso, A., et al. (2013). Journal of Volcanology and Geothermal Research, 261:153-170.
Chiodini , G., et al. (2017). Scientific Reports, 7: 4472.
Cornelius, R. and Voight, B. (1994). Journal of Volcanology and Geothermal Research, 62:469-498.
Cornelius, R. and Voight, B. (1995). Journal of Volcanology and Geothermal Research, 64:295-320.
Cornelius, R. and Voight, B. (1996). Fire and mud: eruptions and lahars of Mount Pinatubo, Philippines.
Cox, D. R., and V. Isham (1980), Point Processes, pp. 188, Chapman and Hall, London and New York.
D'Auria, L., et al. (2011). Journal of Geophysical Research, 116, B04313.
Fukuzuno, T. (1985). Journal of Japanese Landslide Society, 22:8-14.
Hull, J. and White, A. (1990). The Review of Financial Studies, 3:573-592.
Hyman, D. M. et al. (2018). Journal of Geophysical Research: Solid Earth, 123, 8527–8547.
Kilburn, C. R. and Petley, D. N. (2003). Geomorphology, 54(1):21-32.
Kilburn, C. (2012). Journal of Geophysical Research: Solid Earth (1978-2012), 117(B2).
Kilburn, C., et al. (2017). Nature Communications, 8:15312-15319.
Kilburn, C. (2018). Frontiers in Earth Science, 6:133.
Müller, L. (1964). Rock Mechanics and Engineering Geology, 2:148-212.
Ortiz, R., et al. (2003). Journal of Volcanology and Geothermal Research, 128(1):247-259.
Robertson, R. M. and Kilburn, C. R. (2016). Earth and Planetary Science Letters, 438:86-94.
Salvage, R. and Neuberg, J. (2016). Journal of Volcanology and Geothermal Research, 324:118-133.
Swanson, D. A., et al. (1983). Science, 221(4618):1369-1376.
Tokarev, P. (1966). Nauka, USSR Academy of Sciences.
Troise, L., et al. (2019). Earth-Science Reviews, 188:108-122.
Vasseur, J., et al. (2015). Scientic Reports, 453:13259-13265.
Voight, B. (1988), Nature, 332:125-130.
Voight, B. (1989). Science, 243(4888):200-203.
Voight, B. and Cornelius, R. R. (1991). Nature, 350:695-698.
Voight, B., et al. (2000). Journal of Volcanology and Geothermal Research, 100(1):261-287.